



Evaluation of mechanical, optical and thermal properties of PVA nanocomposites embedded with Fe₂O₃ nanofillers and the investigation of their thermal decomposition characteristics under non-isothermal heating condition

V. Parthasarathy¹ · J. Selvi¹ · P. Senthil Kumar² · R. Anbarasan³ · S. Mahalakshmi⁴

Received: 18 November 2019 / Revised: 18 March 2020 / Accepted: 16 April 2020 /

Published online: 7 May 2020

© Springer-Verlag GmbH Germany, part of Springer Nature 2020

Abstract

Magnetic Fe₂O₃ nanopowder was synthesized and characterized by various analytical techniques. The PVA/Fe₂O₃ nanocomposites were prepared by solution casting method to investigate the effect of nanofillers on their physicochemical properties. The analytical tools such as FTIR, UV–visible spectra and XRD were used to analyze the structure of Fe₂O₃ nanopowder and PVA/Fe₂O₃ nanocomposites. The uniform distribution of the Fe₂O₃ nanofillers on the PVA matrix was inspected using SEM. The particle size of the crystalline Fe₂O₃ nanofillers was observed to be less than 30 nm from the TEM micrographs. The optical characteristics of the prepared samples were investigated by analyzing their UV–visible spectra. The bandgap of PVA nanocomposites was lower than for pure PVA due to the dispersed Fe₂O₃ nanofillers in the PVA matrix. The thermal properties of pristine PVA and PVA/Fe₂O₃ nanocomposites were investigated by TGA. The PVA/Fe₂O₃ nanocomposite systems exhibited the improved thermal stability. The thermal degradation mechanism of PVA/Fe₂O₃ nanocomposite system was inspected in depth at five different heating rates under non-isothermal conditions. The electrical and mechanical properties of PVA were enhanced remarkably while increasing the % weight loading of nanopowder.

Keywords PVA · Thermal degradation · Bandgap · Mechanical study · Nanocomposite

✉ V. Parthasarathy
parthu0406@gmail.com

Extended author information available on the last page of the article

Introduction

Poly(vinyl alcohol) (PVA) is a non-toxic, odorless, thermostable, transparent, semicrystalline and linear synthetic biodegradable polymer [1]. The semicrystalline nature of PVA arises due to the existing hydrogen bonds between the PVA chains. PVA has an excellent charge storage ability, optical properties and high dielectric strength. The versatile applications of PVA are in optical sensors, batteries, fuel cell, osmotic power plants, water filtration system, optical devices, biomedical, pharmaceutical and others [2, 3]. Unfortunately, it exhibits poor thermal properties. The thermal, optical, electrical and mechanical properties of PVA can be altered by doping with inorganic nanofillers. $\alpha\text{-Fe}_2\text{O}_3$ (hematite) is a n-type semiconductor, is non-toxic, has thermodynamically stable phase in the ambient condition with the narrow bandgap of approximately 2.1 eV [4] and has high corrosion resistance. The novelty of the present investigation is to improve the thermal stability of PVA, and the same was studied under non-isothermal conditions.

The effect of different wt% of PbS nanofillers on the optical and structural properties of PVA nanocomposite was inspected by Abdullah et al. [5]. This study revealed that PVA/PbS nanocomposites exhibited high UV and visible light absorption due to the addition of PbS nanoparticles. The studies on the thermal property and tensile strength of ZrO_2 -doped PVA nanocomposites were reported in the literature [6]. PVA/PbO nanocomposites were prepared by colloidal processing techniques and their mechanical and dielectric properties were investigated with the different concentrations of PbO nanoparticles [7]. PVA nanocomposites loaded with different concentrations of modified CaCO_3 nanoparticles were investigated to assess their wetting and heavy metal absorption properties [8]. PVA nanocomposites doped with various concentrations of CeO_2 nanofillers were suggested to be used in solar cells and filters due to their good absorption in UV and visible regions [9]. PVA nanocomposites doped with various metal oxide nanoparticles such as In_2O_3 [10] and MnO_2 [11] were investigated to analyze their physicochemical properties and possible technological applications. Wei et al. [12] prepared PVA/antimony-doped tin oxide (ATO) by solution blending method, and the crystallization and glass transition temperatures of PVA were altered after the addition of ATO. The mechanical properties of PVA/ATO nanocomposites were decreased at the higher loading of ATO content as compared with PVA. The effect of the addition of NaNO_3 on the optical properties of PVA/ NaNO_3 nanocomposite systems was examined by Muhammad and his research team [13]. The increase in refractive index and dielectric constant was reported for NaNO_3 -incorporated PVA nanocomposites. The ceramic additive, $\text{EuBa}_2\text{Ca}_2\text{Cu}_{-3}\text{O}_{-9-x}$ -incorporated PVA nanocomposites were examined to assess their thermal and mechanical properties [14]. The dielectric and structural properties of PVA/barium zirconium titanate composites were studied for embedded capacitors application [15]. Shirbeeney et al. investigated the PVA/YBCO nanocomposite to improve the efficiency of solar energy conversion [16]. Zhou and his research team [17] prepared the MoS_2 -doped PVA nanocomposites and analyzed

their enhanced properties associated with the structural characteristics of the nanocomposites. The structural and temperature-dependent dielectric properties of PVA/Al₂O₃ nanocomposites were examined by More et al. [18]. The thermal properties of CdS- and ZnS-embedded PVA nanocomposites were reported in the literature [19].

This study aims to investigate the thermal and thermal decomposition behavior of PVA/Fe₂O₃ nanocomposite using various kinetic models under non-isothermal conditions. It is understood from the literature that the assessment of thermal and thermal degradation behaviors of biodegradable PVA nanocomposites is very essential because such type of polymer composites degrade slightly while processing in industries under non-isothermal conditions. However, there is no report on the thermal decomposition behavior of PVA/Fe₂O₃ nanocomposites under different heating rates. The PVA-based materials find lot of applications in the biomedical field owing to their biocompatible and biodegradable nature. However, the potential applications of these materials are restricted owing to their inadequate mechanical properties in the biomedical field. This work also aims to enhance the mechanical property of PVA by dispersing Fe₂O₃ nanofillers in the PVA matrix. The prepared PVA/Fe₂O₃ nanocomposites can be used in photonic and optoelectronic applications due to their improved thermal and semiconducting nature and also in the biomedical field due to the enhanced mechanical properties.

Experimental

Materials

All the utilized chemicals for this study were of AR grade, and they were used without further purification. PVA (85% hydrolyzed) with a M_w of 1,50,000 g/mol was received from Merck, India. FeCl₃ 6H₂O and sodium hydroxide (<99% purity) were used as the precursor and reducing agent, respectively, for the preparation of Fe₂O₃ nanoparticles, and they were received from SD Fine Chemical, India. All the chemical reactions were carried out only in the double-distilled (DD) water.

Synthesis of iron oxide nanoparticles

The iron oxide (Fe₂O₃) nanopowder was synthesized by a standard co-precipitation method [20] using FeCl₃ 6H₂O as a starting precursor. The aqueous solution of FeCl₃ 6H₂O was prepared by dissolving 2.4 g of iron chloride precursor in 100 mL DD water. The prepared 0.10 N NaOH solution was slowly mixed to the precursor solution under stirring. The reaction proceeds with the formation of a dark brown precipitate. The iron hydroxide precipitate became more turbid while increasing pH. It was continuously stirred for an hour after the completion of the reaction. The precipitate was allowed to settle down at the bottom of the beaker. This iron hydroxide precipitate was separated by filtration and rinsed with distilled water several times to remove the unreacted precursor. The dried substance was crushed into a fine

powder. The fine powder was annealed at 400 °C in a furnace for 2 h to prepare Fe₂O₃ nanoparticles.

Synthesis of PVA/Fe₂O₃ nanocomposite films

PVA nanocomposites were prepared by dispersing the various amounts of Fe₂O₃ nanoparticles in the host PVA matrix. The different concentrations of Fe₂O₃ nanofillers and the predetermined constant weight of PVA were used for the preparation of PVA-based nanocomposites. The clear aqueous solution of PVA was prepared by dissolving the PVA granules (2 g) in 100 mL DD water at 80 °C under constant stirring. Afterward, 2 wt% of Fe₂O₃ nanoparticles was dispersed into the above polymer solution under the same stirring condition. The uniformly dispersed Fe₂O₃ nanofillers within the host polymer matrix were achieved by stirring the mixture overnight. This solution mixture was poured onto polyimide dish to cast it as a thin nanocomposite film. The casting solution was kept at 50 °C for 6 h in vacuum to prepare the bubble-free PVA nanocomposite film. 2 wt% of Fe₂O₃ nanoparticles-doped PVA nanocomposite films was peeled off from the dish to carry out the structural study. The same methodology was employed to fabricate the PVA nanocomposite films loaded with 4 and 6 wt% of Fe₂O₃ nanofillers. The pure PVA film was also prepared by using the same protocol without nanofillers.

Characterization

The influence of Fe₂O₃ nanofillers on the physicochemical properties of PVA nanocomposites and also the structure–property relation of nanocomposites was analyzed using various analytical techniques. The structural analysis was performed on a Shimadzu 8400S FTIR spectrophotometer, Japan, in the spectral range of 400–4000 cm⁻¹ for all the Fe₂O₃ nanoparticles and PVA nanocomposite films. The structural determination was further carried out by scanning the samples with Cu K- α radiation of wavelength 1.5406 Å in the range of 20°–80° at 2 θ scale using a Bruker D8 advanced X-ray diffractometer. The chemical structure and crystalline phase of the samples were authentically confirmed by analyzing their XRD patterns. The grain size (d) of the Fe₂O₃ nanofillers was evaluated using Scherer's formula as in Eq. 1 [18]:

$$d = \frac{0.94\lambda}{\beta \cos \theta} \quad (1)$$

where d and θ denote the average crystallite size and diffraction angle, respectively, β FWHM and λ wavelength of the X-rays.

The optical characteristics of the Fe₂O₃ nanofillers and PVA nanocomposite systems were examined by exposing the samples to UV–visible light in the wavelength range of 200–800 nm using a UV-1800 Shimadzu spectrophotometer. The variation in the light absorption behavior of the polymer samples was investigated by analyzing their UV–visible spectra. The effect of the addition of nanofillers on the bandgap value of PVA was inspected using Tauc's relation as in Eq. (2) [21]:

$$ahv = A(hv - E_g)^n \tag{2}$$

where absorption coefficient α , photon energy $h\nu$ and n denote the types of transition depending on the values of n (1/2, 3/2, 2 and 3). The morphological observation was done with the help of Hitachi S-3700 N SEM, Germany, for all the samples. The thermal property and thermal decomposition characteristics were analyzed under different heat flows for the prepared PVA/Fe₂O₃ nanocomposite films using a SII 6300 ExSTAR thermal analyzer in an air atmosphere at five different heating rates in the heating range of 30–700 °C.

The DC conductivity study was carried out for pure PVA and PVA nanocomposites using the four-probe (Keithley 617) method at 30 °C. The DC conductivity was calculated for all the polymer samples using the following expression:

$$\sigma_{DC} = \frac{d}{RS} \text{ (s/cm)}$$

where d is the sample thickness, R sample resistance and A area of the electrode.

The mechanical properties of the polymer samples were measured by a universal tensile tester, Deepak Polyplast, India (ASTM D3039/D3039M-17).

Non-isothermal degradation kinetics

The thermal decomposition process of the PVA nanocomposite was examined using the various kinetic models. The activation energy (E_a) for the thermal decomposition process of nanocomposite was computed to assess their thermal decomposition characteristics more accurately. The reaction conversion (α) can be determined by the following expression:

$$\alpha = (W_o - W_t) / (W_o - W_f)$$

where W_o is the initial weight, W_t weight at any prescribed temperature and W_f final sample weight.

In Flynn–Wall–Ozawa (FWO) method [22], the decomposition temperature (T_d) is measured possibly for the fixed value of α under different heating rates. The E_a can be determined for the decomposition process without knowing the reaction order and mechanism by this model. This model also proposes an equation to determine E_a as follows:

$$\log\beta = 1 + \log \frac{AEa}{Rg(a)} - 2.315 - 0.4567 \frac{Ea}{RT} \tag{3}$$

where T is the temperature, β heating rate and R gas constant.

The Kissinger model proposes that the reaction extent (α) is maximum, only at the degradation temperature (T_d) [23]. The reaction extent is always constant at T_d according to this model. Though, it may vary with the heating rate.

$$\ln \left(\frac{\beta}{T_d^2} \right) = \ln \left(\frac{AR}{E} \right) - \frac{E}{RT_d}. \quad (4)$$

The Auggis–Bennet model is also used to estimate E_a for the degradation of PVA nanocomposite film [24]. The proposed mathematical expression is in Eq. 5:

$$\ln \left(\frac{\beta}{T_d} \right) = \frac{E}{RT_d} + \ln A. \quad (5)$$

The Friedman model is also applied to understand the degradation mechanism under various heating rates [22]. This model had been modified using certain assumptions put forth by other iso-conversional expressions for some differential applications. The mathematical expression proposed by this model is in Eq. 6:

$$\ln \left(\frac{d\alpha}{dt} \right) = \ln [Qaf(a)] - \frac{E_a}{RT} \quad (6)$$

where R is the gas constant, Q released heat, α conversion rate and T temperature.

The estimation of E_a is also carried out using the model-free method. Kissinger–Akahira–Sunose (KAS) is also called as an iso-conversional method. The accurate E_a value can be estimated by plotting a graph between $d\alpha/dt$ versus temperature by this model. The suggested mathematical expression is in Eq. 7 [23]:

$$\ln \left(\frac{\beta}{T_d^2} \right) = \text{Const} - \frac{(E_a)_\alpha}{RT_\alpha}. \quad (7)$$

Results and discussion

FTIR analysis

Figure 1a displays the FTIR spectrum of Fe_2O_3 nanopowder. A narrow peak at 525 cm^{-1} is attributed to metal oxide (M–O) stretching. The presence of M–O stretching authentically proves the formation of Fe_2O_3 NPs. Figure 1b–e illustrates the FTIR spectra of pure PVA and its nanocomposites. The peaks associated with the structure of PVA are illustrated here. A broad band at 3266 cm^{-1} is related to hydroxyl stretching (O–H) of host PVA matrix. A peak at 2915 cm^{-1} is observed to be C–H asymmetric stretching. A narrow peak at 1731 cm^{-1} is related to carbonyl stretching (C=O) of the acetyl group of PVA. The peaks of $-\text{CH}_2$ bending and wagging vibrations are seen at 1427 cm^{-1} and 1368 cm^{-1} , respectively. A peak at 1247 cm^{-1} is related to C–O–C stretching of the host matrix. The peak at 833 cm^{-1} is associated with $-\text{CH}_2$ stretching vibration of PVA. The above-discussed peaks are also present for the prepared PVA nanocomposites [Fig. 1c–e]. The interaction of Fe_2O_3 nanofillers with the polymer matrix is authentically confirmed by the presence of M–O stretching peak at 520 cm^{-1} . This peak was not observed for pristine

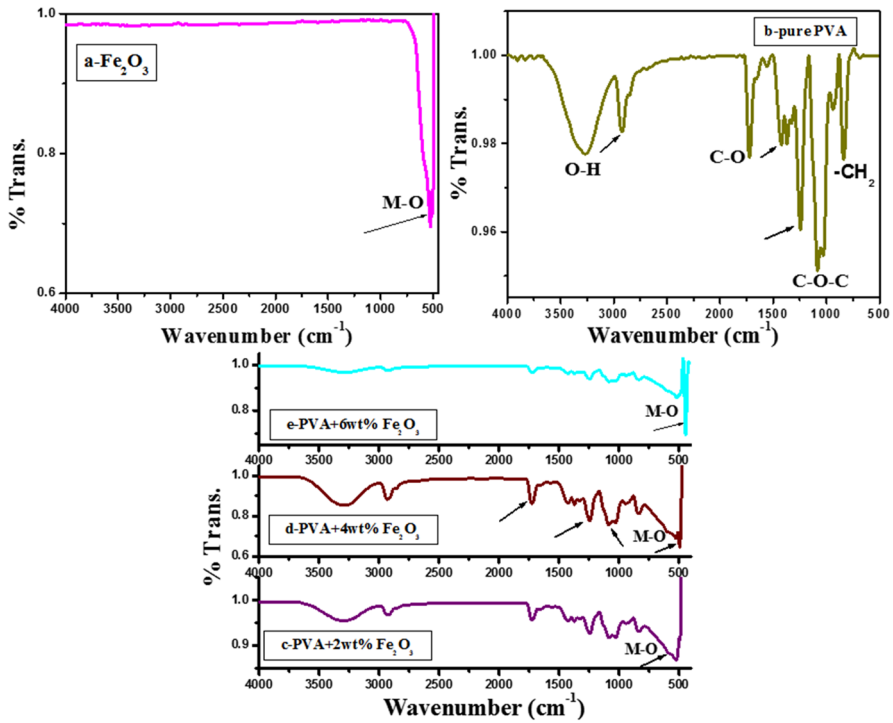


Fig. 1 FTIR spectra of: **a** Fe_2O_3 nanofillers; **b** pristine PVA; **c–e** PVA– Fe_2O_3 nanocomposites

PVA. The charge transfer complex can be formed by the interaction of hydroxyl group of PVA with Fe_2O_3 nanofillers through chelation [25].

XRD study

The prepared Fe_2O_3 nanopowder was analyzed using XRD to identify its chemical structure and determine the grain size. The XRD pattern of Fe_2O_3 nanopowder is portrayed in Fig. 2a. The broadness in the diffraction peaks confirming the particle size of the Fe_2O_3 powder is in the nanorange. The synthesized Fe_2O_3 powder is crystalline in nature which is proved by the appearance of the distinct sharp peaks. The assigned diffraction peaks of Fe_2O_3 nanopowder at the 2θ values of 24.3° (012), 33.1° (104), 35.8° (110), 41° (113), 49.4° (024), 54.1° (116), 57.5° (018), 62.4° (214) and 64.2° (300) are well matched with JCPDS card no. 24-0072 [26]. The diffraction peaks also suggested the rhombohedral phase of Fe_2O_3 nanoparticles. The average grain size of Fe_2O_3 nanopowder was evaluated as 28 nm using Eq. 1. Figure 2b illustrates the XRD profile of pristine PVA. A characteristic peak at 2θ value of 19.8° (101) is attributed to the semicrystalline nature of PVA [27]. There is no more peak in the XRD pattern of pristine PVA. The structure of PVA nanocomposites embedded with various concentrations of Fe_2O_3 was also investigated

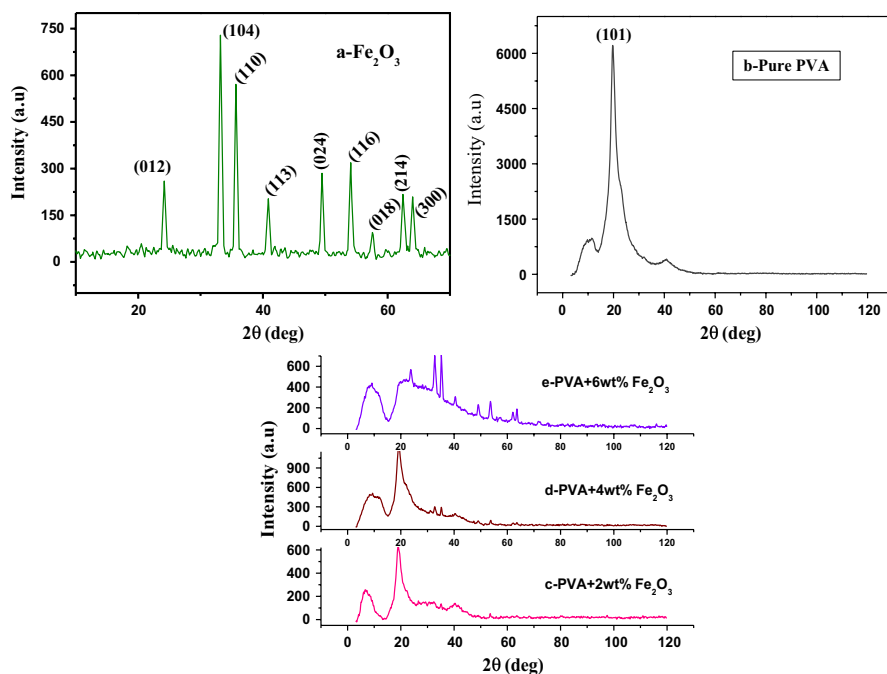


Fig. 2 XRD patterns of **a** Fe_2O_3 nanofillers, **b** pristine PVA, **c–e** PVA– Fe_2O_3 nanocomposites

by analyzing their XRD patterns (Fig. 2c–e). The XRD patterns of the nanocomposite films are comprised of both (101) peak of pure PVA and the crystalline peaks of Fe_2O_3 nanoparticles. Hence, the physical interaction of Fe_2O_3 with PVA matrix is understood from the XRD results. However, the semicrystalline nature of PVA was suppressed after the addition of crystalline Fe_2O_3 nanoparticles for 6 wt% Fe_2O_3 -doped PVA nanocomposites.

Surface morphology using SEM

The morphology of the Fe_2O_3 nanopowder was investigated using SEM. Figure 3a shows the SEM micrograph of Fe_2O_3 nanopowder. All the grains are seen to be agglomerated due to high surface energy. Moreover, the grains exhibit porous structure and the size and size distribution of grains are homogeneous in the SEM illustration. Figure 3b represents the SEM micrograph of pristine PVA film. The film looks very dark without any voids. It confirms that the casted film has no air bubbles. The surface morphology of the Fe_2O_3 nanofiller-incorporated PVA nanocomposites was also investigated to comprehend the physical interaction of Fe_2O_3 nanofiller with the polymer matrix. The SEM micrographs of polymer nanocomposite films are given in Fig. 3c–e. All the composite films are seen embedded with Fe_2O_3 NPs in their matrix as compared with pristine PVA film. It also confirms the interaction of Fe_2O_3 nanofillers with the PVA matrix. However, the NPs start agglomerating

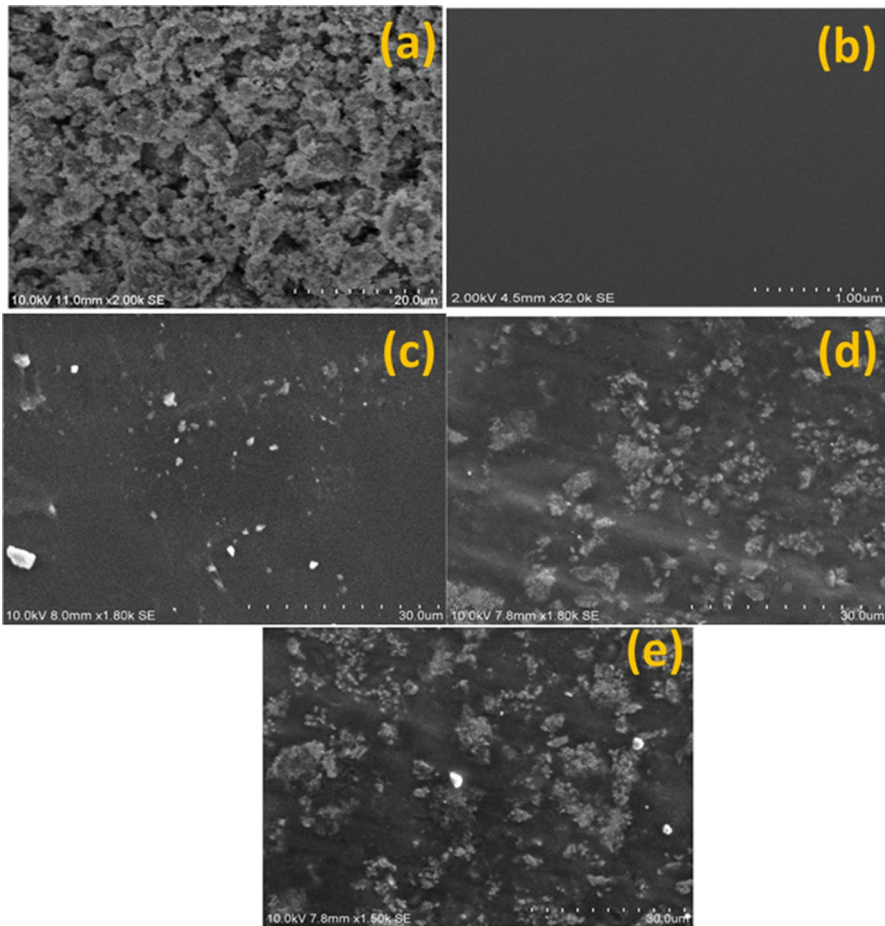


Fig. 3 SEM images of **a** Fe₂O₃ nanofillers, **b** pure PVA, **c** 2 wt% Fe₂O₃-doped PVA nanocomposite, **d** 4 wt% Fe₂O₃-doped PVA nanocomposite, **e** 6 wt% Fe₂O₃-doped PVA nanocomposite

while increasing the concentration of Fe₂O₃. The reason for the uniform dispersion of Fe₂O₃ nanofillers at lower concentration without any agglomeration is due to the mobility of the nanofillers which gets hindered in the viscous PVA matrix. However, the agglomeration of NPs in the PVA matrix is unavoidable at higher concentration owing to their high surface energy [28]. All the polymer nanocomposite films were casted without any air bubbles, which can be observed from the micrographs.

TEM analysis

The prepared Fe₂O₃ nanopowder was examined to analyze its morphology and particle size using TEM. Figure 4a demonstrates the HRTEM image of Fe₂O₃ nanopowder. The grains are interlinked with each other. The grain morphology seems to

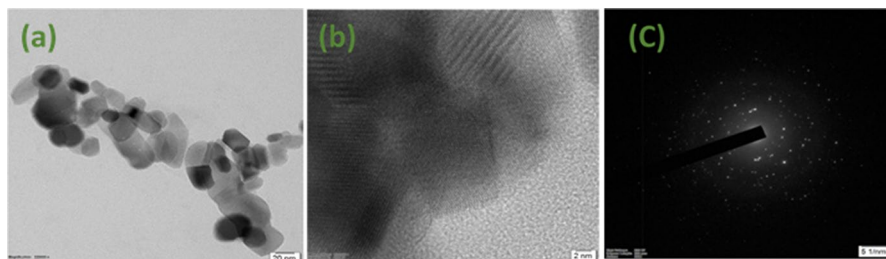


Fig. 4 **a, b** HRTEM images of Fe_2O_3 nanofillers, **c** SEAD pattern of Fe_2O_3 nanofillers

be irregular in shape. The particle size of the Fe_2O_3 nanofillers is found to be less than 30 nm. The layered structure of the micrograph reveals the crystalline nature of Fe_2O_3 nanopowder (Fig. 4b). The SEAD pattern of Fe_2O_3 nanopowder is depicted in Fig. 4c. The reason for the concentric circles with bright spots in the SEAD pattern is the reflection from the highly ordered atomic arrangement of Fe_2O_3 nanopowder. It further confirms the crystalline nature of Fe_2O_3 nanopowder. Hence, the HRTEM results are coinciding well with the XRD patterns.

UV–Visible spectroscopy

Figure 5a illustrates the UV–Visible spectrum of Fe_2O_3 nanopowder. A peak at 356 nm is attributed to the direct transition of Fe_2O_3 . The energy bandgap (E_g) value of Fe_2O_3 nanopowder was determined using optical absorption coefficient (α). The absorption coefficient is used to examine the electronic band structure and the bandgap of the materials. A graph was drawn between $(\alpha h\nu)^2$ and $h\nu$ to evaluate the direct bandgap value of Fe_2O_3 as illustrated in Fig. 5b. The bandgap (E_g) of Fe_2O_3 nanopowder was computed as 3.42 eV by the extrapolation method. The E_g value is

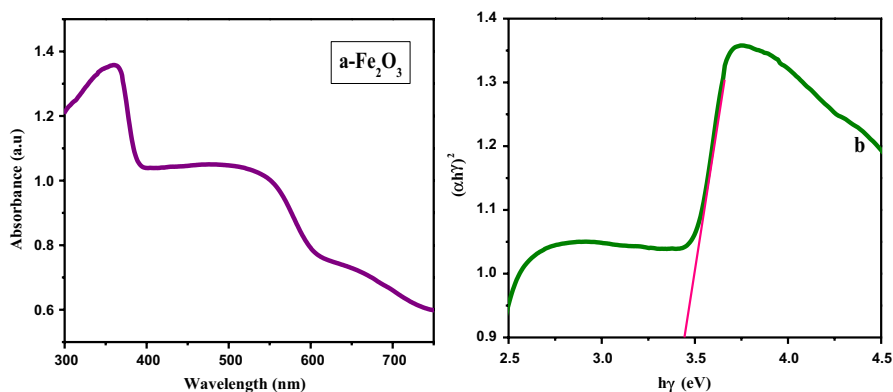


Fig. 5 **a** UV–visible absorption spectrum of Fe_2O_3 nanofillers, **b** bandgap of Fe_2O_3 nanofillers for direct allowed transition

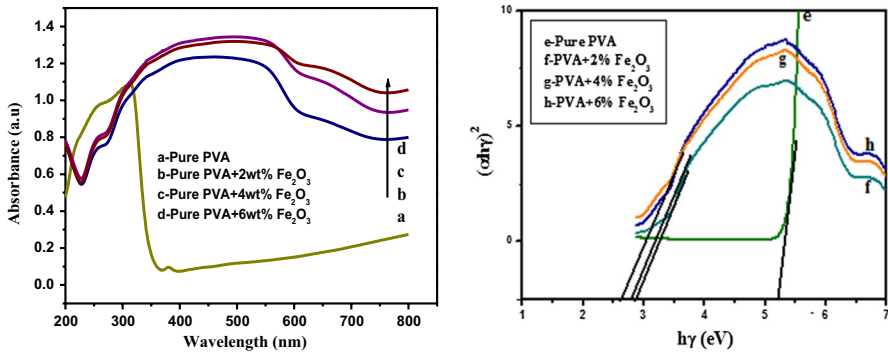


Fig. 6 UV-visible absorption spectra of **a** pure PVA, **b–d** PVA nanocomposite films, optical energy gap of **e** pure PVA, **f–h** PVA nanocomposite films

higher as compared with bulk Fe_2O_3 . The increase in the bandgap of Fe_2O_3 nanopowder is due to quantum confinement effect. The UV–Vis spectra of PVA and its nanocomposites loaded with 2, 4 and 6 wt% of Fe_2O_3 are illustrated in Fig. 6a–d. The absorptions at 255 nm ($\pi\text{-}\pi^*$ transition) and 311 nm ($n\text{-}\pi^*$ transition) are related to pure PVA [28]. The shift in the absorption peaks to higher wavelength confirms the formation of PVA/ Fe_2O_3 nanocomposite films. The rate of absorbance for the nanocomposite films was gradually increased in accordance with Fe_2O_3 nanofillers content in the host PVA matrix. The free electrons of the incorporated Fe_2O_3 nanofiller had absorbed some excess light radiation, which leads to higher absorption for the nanocomposite films. The effect of the incorporated Fe_2O_3 nanofillers on the bandgap of PVA was also investigated by plotting a graph between $(\alpha h\nu)^2$ and $h\nu$ as shown in Fig. 6e–h. The decrease in bandgap (E_g) of pure PVA was noticed after the addition of different wt% of Fe_2O_3 nanofillers in the PVA matrix (Table 1). The incorporated Fe_2O_3 nanofillers had created new energy states in the forbidden gap of PVA, which led to a decrease in the bandgap.

TGA study

The thermal stability of the polymeric materials is generally assessed by a thermogravimetric analyzer. The TG thermograms of PVA and PVA nanocomposites embedded with different weight % of Fe_2O_3 nanofillers heated at 10 °C/min are

Table 1 Direct bandgap value of PVA and its nanocomposites

Sample	Direct bandgap (eV)
Pristine PVA	5.10
PVA + 2 wt% Fe_2O_3	2.92
PVA + 4 wt% Fe_2O_3	2.84
PVA + 6 wt% Fe_2O_3	2.71

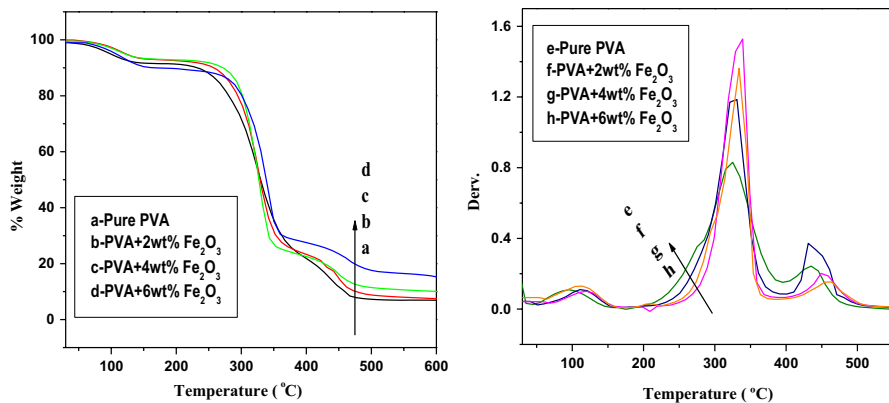


Fig. 7 TG thermograms of **a** pure PVA and **b–d** PVA nanocomposite films heated at $10\text{ }^{\circ}\text{C min}^{-1}$; DTG thermograms of **(e)** pure PVA and **f–h** PVA nanocomposite films heated at $10\text{ }^{\circ}\text{C min}^{-1}$

shown in Fig. 7a–d. It is noted that the degradation process of PVA and PVA nanocomposites has occurred in three steps. The first minor weight loss step occurs at $52\text{ }^{\circ}\text{C}$ for pure PVA and it is occurred in the range of $68\text{--}83\text{ }^{\circ}\text{C}$ for PVA nanocomposites. This is associated with the dehydration of PVA. The second weight loss step begins at $181\text{ }^{\circ}\text{C}$ for pristine PVA and it is started in the range of $212\text{--}237\text{ }^{\circ}\text{C}$ for PVA nanocomposites. This weight loss is attributed to the elimination of water produced by the acetyl groups, acetic acid and non-conjugated polyenes for pure PVA. For the PVA nanocomposite films, the weight loss proceeds with the chain scission reactions associating with the liberation of acetone, acetaldehyde and furan [29]. The third weight loss begins at $401\text{ }^{\circ}\text{C}$ for host PVA matrix and it is occurred in the range of $406\text{--}417\text{ }^{\circ}\text{C}$ for PVA nanocomposites. This weight loss is associated with the complete degradation of the PVA backbone. It is found that the degradation steps are increased on increasing the Fe₂O₃ nanofillers contents in the host PVA matrix. The maximum degradation temperature (T_d) of PVA nanocomposites doped with various wt% of Fe₂O₃ nanofillers occurs in the range of $105.7\text{--}138\text{ }^{\circ}\text{C}$ for step I, $335\text{ }^{\circ}\text{C}$ to $355\text{ }^{\circ}\text{C}$ for step II and $441\text{ }^{\circ}\text{C}$ to $461\text{ }^{\circ}\text{C}$ for step III degradation processes. The T_d values of PVA nanocomposites are higher than those of PVA. The results of the TG thermograms conclude that there is an enhancement in the thermal stability of PVA nanocomposites as compared with pure PVA. The DTG thermograms of all the prepared samples also conclude the same as shown in Fig. 7e–f.

Non-isothermal degradation study

The thermal degradation mechanism of PVA nanocomposite doped with 4 wt% of Fe₂O₃ nanofillers is examined under non-isothermal heating (from 10 to $30\text{ }^{\circ}\text{C/min}$ in steps of $5\text{ }^{\circ}\text{C/min}$) in the temperature range of $30\text{--}700\text{ }^{\circ}\text{C}$. The TG thermograms recorded at five heating rates for the PVA nanocomposite with 4 wt% nanofiller loading are portrayed in Fig. 8a–e. The thermal decomposition occurs in three steps under non-isothermal heating for this sample. However, there is a shift

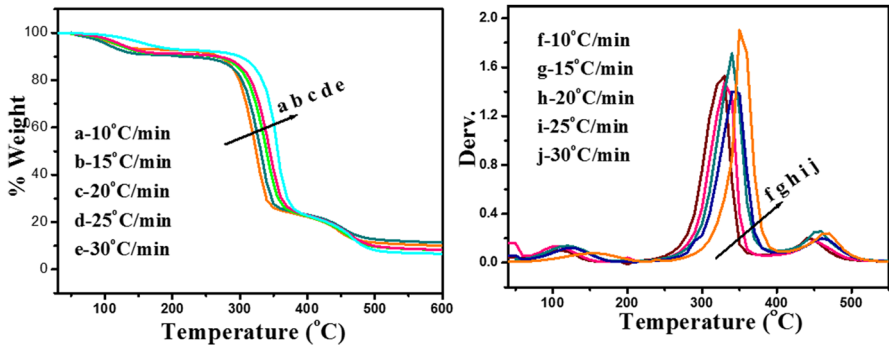


Fig. 8 a–f TG thermograms of PVA nanocomposite and f–j DTG thermograms of PVA nanocomposite

in the degradation temperature toward higher temperature on increasing the heating rate [23]. The DTG thermograms recorded at five heating rates for the PVA nanocomposite are depicted Fig. 8f–j. All the DTG thermograms show three exothermic peaks with a shift in their peak position. It also confirms the three-step degradation processes of the sample and the increase in T_d with an increase in heat flow. The increase in T_d is also concluded from the plot of T_d versus temperature (Fig. 9a–c).

The decomposition of the sample is associated with the consumption of heat energy. The accurate determination of activation energy (E_a) associating with the degradation process is more useful to process the polymeric materials in industries under non-isothermal heating. Hence, the various kinetic models have been employed in determining the E_a values for the prepared sample. A graph is plotted between $\ln(\beta)$ and $1000/T_d$ for FWO (Fig. 10a, d, f), $\ln(\beta/T_d)$ versus $1000/T_d$ for Auggis–Bennet (Fig. 10b, e, h) and $\ln(\beta/T_d^2)$ versus $1000/T_d$ for Kissinger models (Fig. 10c, f, i), respectively, to determine E_a by linear fit method. The E_a value is

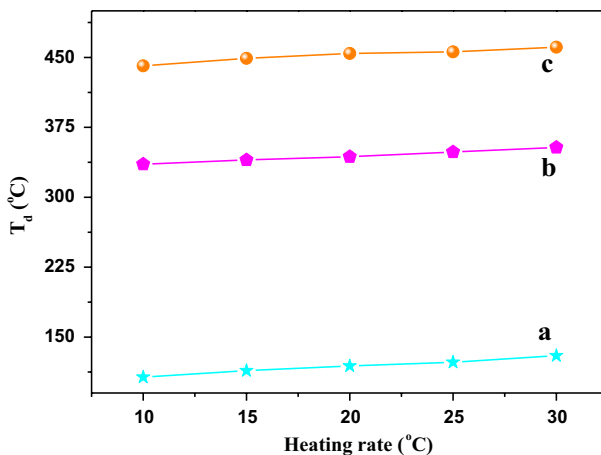


Fig. 9 The plots of heating rate versus degradation temperature for a step I, b step II and c step III for PVA nanocomposite

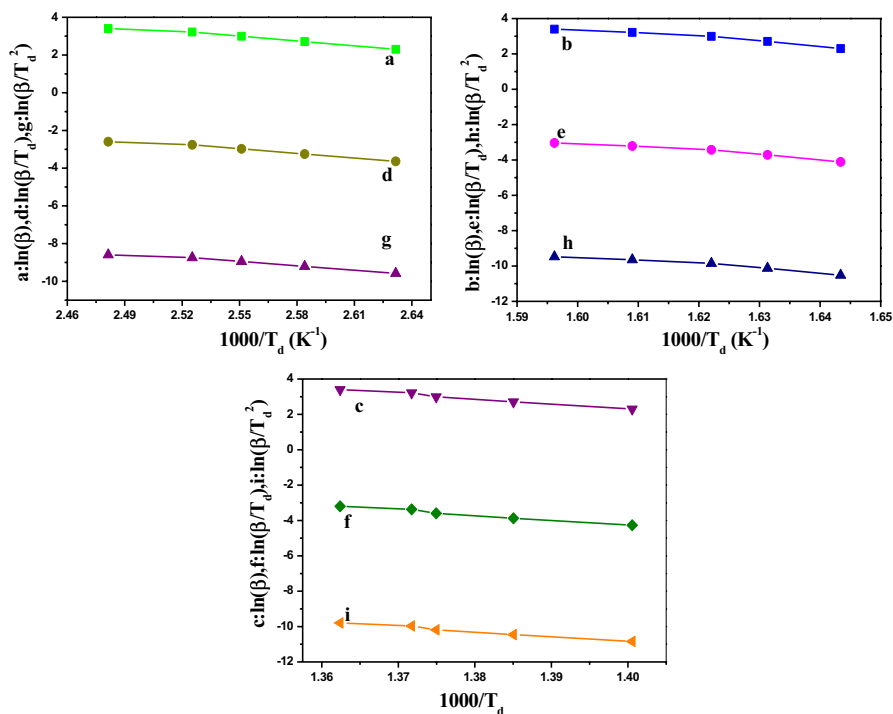


Fig. 10 The classical plots of: **a–c** Flynn–Wall–Ozawa model, **d–f** Auggis–Bennet model and **g–i** Kissinger model for step I, step II and step III for PVA–Fe₂O₃ nanocomposite

Table 2 Energy of activation (E_a) related to the thermal degradation of PVA nanocomposite embedded with 4 wt% Fe₂O₃ nanofiller

Kinetic models	Step I	Step II	Step III
	E_a kJ/mol	E_a kJ/mol	E_a kJ/mol
FWO	66.2	191.2	246.2
Auggis–Bennet	62.9	186.0	240.0
Kissinger	59.7	180.9	234.0

higher for stage II than for stage I due to the minor decomposition process. It is also higher for stage III as compared with remaining stages (I and II) due to the major decomposition of the PVA backbone. The Kissinger model yields a lower E_a value than other models. The E_a values are given in Table 2.

The Friedman model is also employed in determining the E_a values associating with the decomposition of the nanocomposite sample. A graph is plotted between $\ln(d\alpha/dt)$ and $1/T$ to compute the E_a values associating with three stages. A decreasing trend is observed from all the three plots as illustrated in Fig. 11a–e, f–j and k–o, respectively. The E_a values (46 to 66 kJ mol⁻¹) are lower for stage I as compared with stage II (172.3 to 195 kJ mol⁻¹). Moreover, the E_a values (211 to 251 kJ mol⁻¹) of stage III are comparatively higher than those of stages I and

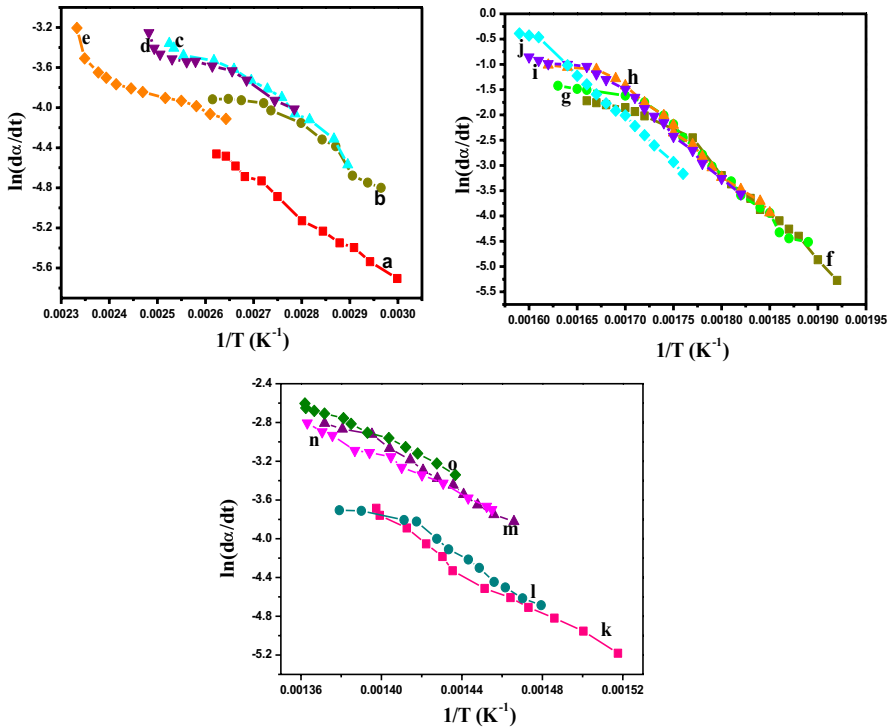


Fig. 11 The Friedman plots of: **a–e** stage I, **f–j** stage II and **k–o** stage III degradation for PVA–Fe₂O₃ nanocomposite

II. The Friedman model is also consistent with other models as compared with the obtained E_a values for all the five heating rates. The E_a value was reported as higher for PVA/silica nanocomposites than that of pure PVA by Peng et al. [29]. The present PVA nanocomposite system also exhibits higher E_a value in accordance with the reported system.

KAS method is known to be an iso-conversional method. It is very essential to understand the variation in reaction extent as a function of temperature to employ this model. The increase in T_d with an increase in heat flow is understood from the plot of reaction extent (α) versus temperature as illustrated in Fig. 12a–e. The decrease in reaction extent with an increase in heat flow is also noted [24]. The variation of $d\alpha/dt$ versus temperature is understood from Fig. 12f–j. The derivative of reaction extent increases with an increase in heat flow. The E_a values are also determined for the PVA nanocomposite using KAS model. The plot of E_a versus α is depicted in Fig. 12k–o. There is a slight increase in E_a values with the reaction extent. The variation in the E_a values is from 72.5 to 192.9 kJ mol⁻¹ at $\alpha=0.5$ and 84.2 to 238.3 kJ mol⁻¹ at $\alpha=1$ for different heating rates. This is because of the rate limiting steps of random chain scission process [22].

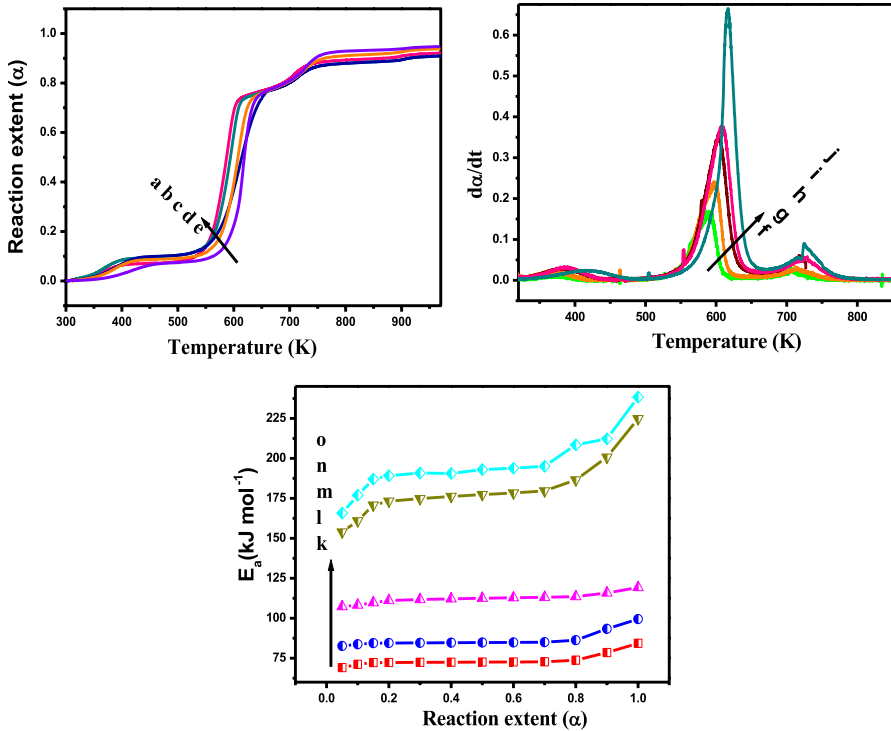


Fig. 12 The plots of: **a–e** α versus temp, **f–j** derivative of $d\alpha/dt$ versus temperature and **k–o** E_a versus reaction extent by KAS method at different heating rates

Mechanical properties

The mechanical studies are carried out for all the prepared samples (PVA and 2, 4 & 6 wt% of Fe_2O_3 nanofillers-embedded PVA nanocomposites) to investigate their mechanical properties. The stress–strain diagram of all the samples is illustrated in Fig. 13a–d. The mechanical parameters such as tensile strength, % elongation and Young's modulus are investigated to understand the mechanical properties of the PVA nanocomposites (Table 3). The tensile strength of pristine PVA is measured to be 85.2 MPa for pristine PVA, which is observed to be low as compared with the tensile strength of PVA nanocomposites films. The tensile strength of PVA increases gradually on increasing the concentration of Fe_2O_3 nanofillers. This is mainly due to the uniform dispersion of Fe_2O_3 nanofillers and also the strong interaction between the hydroxyl group (O–H) of PVA and Fe_2O_3 nanofillers. The present PVA nanocomposite systems yielded better mechanical property than the reported system [30]. The Young's modulus (Y) of PVA is also increased on increasing the Fe_2O_3 nanofillers content. The applied load can be transferred effectively by the dispersed Fe_2O_3 nanofillers in the PVA matrix, resulting in that there is an enhancement in Young's modulus [31]. However, the

Fig. 13 Stress–strain curves of: **a** Pure PVA; **b** PVA + 2 wt% Fe₂O₃; **c** PVA + 4 wt% Fe₂O₃; **d** PVA + 6 wt% Fe₂O₃

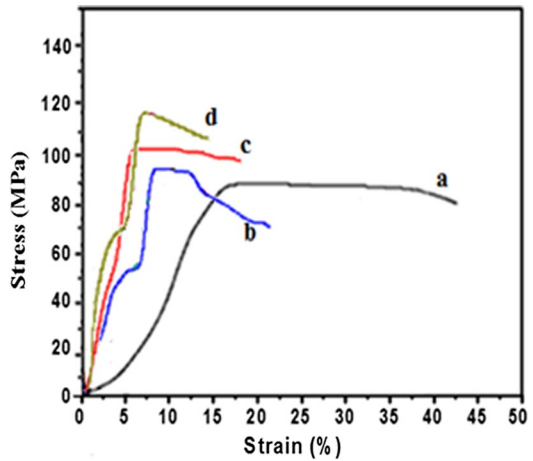


Table 3 Mechanical properties of PVA and PVA/Fe₂O₃ nanocomposites

Sample	Tensile strength (MPa)	Elongation at break (%)	Young's modulus (GPa)
Pure PVA	85.2	39.8	1.4
PVA + 2 wt% Fe ₂ O ₃	97.8	21.5	5.5
PVA + 4 wt% Fe ₂ O ₃	107.2	18.4	8.3
PVA + 6 wt% Fe ₂ O ₃	117.4	14.6	11.1

% elongation at break is reduced on increasing the Fe₂O₃ nanofillers concentration in the host matrix. This is in good agreement with Galil and co-workers [32]. All the values associated with the above analysis are given in Table 3.

DC conductivity analysis

The DC electrical conductivity of PVA and its nanocomposites was examined at room temperature by using the four-probe method. The plot of electrical conductivity versus % wt loading of Fe₂O₃ nanofillers is displayed in Fig. 14. The DC electrical conductivity of PVA was improved after the addition of Fe₂O₃ nanofillers. It was concluded that the incorporated Fe₂O₃ nanofillers had created the conducting paths through a newly introduced charge transfer complexes within the PVA matrix, which led to an increase in conductivity [33].

Conclusion

The influence of Fe₂O₃ nanofillers on the various properties of PVA nanocomposites was successfully investigated. The interaction of Fe₂O₃ nanofillers with the PVA matrix was proved by the assigned metal oxide stretching peak (520 cm⁻¹) in the

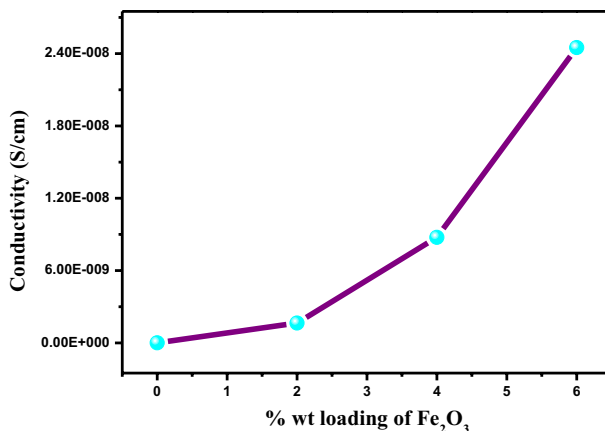


Fig. 14 DC electrical conductivity of PVA and PVA–Fe₂O₃ nanocomposite films

FTIR spectra. The structural confirmation for the prepared PVA nanocomposites was also made by analyzing their XRD profiles. The physical interaction of Fe₂O₃ nanofillers with the PVA and the uniform distribution of Fe₂O₃ nanofillers in the host PVA matrix were confirmed by analyzing the SEM micrographs of PVA nanocomposites. The particle size of Fe₂O₃ nanopowder was determined to be less than 30 nm by TEM. There is the gradual increase in absorption on increasing the concentration of Fe₂O₃ nanofillers for the prepared nanocomposites. The bandgap of PVA was remarkably decreased from 5.1 to 2.71 eV, respectively, after dispersing the nanofillers in the host PVA matrix. The PVA nanocomposite showed better thermal stability than pristine PVA. The shift in the degradation temperature (T_d) toward higher temperature with an increase in heat flow was observed for the prepared nanocomposite system. The E_a values obtained from the five different models are more or less consistent with each other. The Young's modulus (Y) and tensile strength of PVA were increased from 1.4 to 11.1 GPa and from 85.2 to 117.4 MPa after dispersing the nanofillers. The electrical conductivity of PVA nanocomposites was increased and also shifted to the semiconducting regime on increasing the concentration of Fe₂O₃ nanofillers. The PVA/Fe₂O₃ nanocomposite can be used in optoelectronic applications due to its semiconducting nature and in the biomedical field due to the enhanced mechanical properties.

References

1. Abdullah Z, Dong Y, Davies I, Barbhuiya S (2017) PVA, PVA blends, and their nanocomposites for biodegradable packaging application. *Polym Plast Tech Eng* 56:1307–1344
2. Surkatti R, El-Naas M (2014) Biological treatment of wastewater contaminated with p-cresol using *Pseudomonas putida* immobilized in polyvinyl alcohol (PVA) gel. *J Water Process Eng* 1:84–90
3. Saini I, Sharma A, Dhiman R, Aggarwal S, Ram S, Sharma P (2017) Grafted SiC nanocrystals: for enhanced optical, electrical and mechanical properties of polyvinyl alcohol. *J Alloys Compd* 714:172–180

4. Hao C, Shen Y, Wang Z (2015) Preparation and characterization of Fe_2O_3 nanoparticles by solid-phase method and its hydrogen peroxide sensing properties. *ACS Sustain Chem Eng* 4:1069–1077
5. Abdullah O, Tahir D, Kadir K (2015) Optical and structural investigation of synthesized PVA/PbS nanocomposites. *J Mater Sci Mater Elect* 26:6939–6944
6. Krishnamoorthy K, Natarajan S, Kim J, Kadarkaraithangam J (2011) Enhancement in thermal and tensile properties of ZrO_2 /Poly (Vinyl Alcohol) Nanocomposite Film. *Mater Express* 1:329–335
7. Pasha S, Deshmukh K, Ahamed M, Chidambaram K, Mohanapriya M, Raj N (2015) Investigation of microstructure, morphology, mechanical, and dielectric properties of PVA/PbO nanocomposites. *Adv Polym Technol* 36:352–361
8. Mallakpour S, Khadem E (2017) Poly (vinyl alcohol)/ CaCO_3 -diacid nanocomposite: investigation of physical and wetting properties and application in heavy metal adsorption. *J Appl Polym Sci* 134:45414
9. Hemalatha K, Rukmani K (2016) Synthesis, characterization and optical properties of polyvinyl alcohol–cerium oxide nanocomposite films. *RSC Adv* 6:74354–74366
10. Singhal A, Kaur M, Dubey K (2012) Polyvinyl alcohol– In_2O_3 nanocomposite films: synthesis, characterization and gas sensing properties. *RSC Adv* 2:7180–7189
11. Roy H, Mollah M, Islam M, Susan M (2018) Poly (vinyl alcohol)– MnO_2 nanocomposite films as UV-shielding materials. *Polym Bull* 75:5629–5643
12. Wei P, Xiaowei H, Yan C (2010) Preparation and characterization of poly (vinyl alcohol)/antimony-doped tin oxide nanocomposites. *Int J Polym Mater* 60:223–232
13. Mısırlıoğlu B, Özdemir Z, Aksakal B, Salt Y, Tırnakçı B, Denктаş C (2018) Polyvinyl alcohol/ $\text{EuBa}_2\text{Ca}_2\text{Cu}_3\text{O}_{9-x}$ composites: dielectric and mechanical properties. *J Inorg Organomet Polym Mater* 28:1968–1979
14. Muhammad F, Aziz S, Hussein S (2014) Effect of the dopant salt on the optical parameters of PVA: NaNO_3 solid polymer electrolyte. *J Mater Sci Mater Elect* 26:521–529
15. Badapanda T, Senthil V, Anwar S, Cavalcante L, Batista N, Longo E (2013) Structural and dielectric properties of polyvinyl alcohol/barium zirconium titanate polymer–ceramic composite. *Curr Appl Phys* 13:1490–1495
16. Shirbeeney W, Hafez M, Mahmoud W (2013) Synthesis and characterization of PVA/YBCO nanocomposite for improvement of solar energy conversion. *Polym Compos* 34:587–591
17. Zhou K, Jiang S, Bao C (2012) Preparation of poly (vinyl alcohol) nanocomposites with molybdenum disulfide (MoS_2): structural characteristics and markedly enhanced properties. *RSC Adv* 2:11695–11703
18. More S, Dhokne R, Moharil S (2017) Structural properties and temperature dependence dielectric properties of PVA– Al_2O_3 composite thin films. *Polym Bull* 75:909–923
19. Osuntokun J, Ajibade P (2016) Morphology and thermal studies of zinc sulfide and cadmium sulfide nanoparticles in polyvinyl alcohol matrix. *Physica B* 496:106–112
20. Valášková M, Tokarský J, Pavlovský J, Prostějovský P, Kocí K (2019) $\alpha\text{-Fe}_2\text{O}_3$ nanoparticles/Vermiculite clay material: structural, optical and photocatalytic properties. *Materials* 12:1–16
21. Selvi J, Mahalakshmi S, Parthasarathy V (2017) Synthesis, structural, optical, electrical and thermal studies of poly (vinyl alcohol)/CdO nanocomposite films. *J Inorg Organomet Polym Mater* 27:1918–1926
22. Mahalakshmi S, Parthasarathy V, Alagesan T, Anbarasan R (2019) Non-isothermal crystallization and degradation kinetic studies of synthesized Mo-TG end capped poly(ϵ -caprolactone). *Macromol Res* 27:386–395
23. Mahalakshmi S, Parthasarathy V, Tung K, Anbarasan R, Alagesan T (2019) Non-isothermal crystallization and degradation kinetics of Fe_3O_4 –thymolblue functionalized poly(ϵ -caprolactone). *J Polym Environ* 27:1259–1272
24. Mahalakshmi S, Alagesan T, Parthasarathy V, Tung K, Anbarasan R (2019) Crystallization and degradation kinetics studies on Cu-TG functionalized poly(ϵ -caprolactone) by non-isothermal approach. *J Polym Res* 26(6):50
25. Rao J, Raizada A, Ganguly D, Mankad M, Satyanarayana S, Madhu G (2015) Enhanced mechanical properties of polyvinyl alcohol composite films containing copper oxide nanoparticles as filler. *Polym Bull* 72:2033–2047
26. Fu Y, Zhang H, Chen J (2001) Synthesis of Fe_2O_3 nanowires by oxidation of iron. *Chem Phys Lett* 350:491–494

27. Rao J, Raizada A, Ganguly D, Mankad M, Satyanarayana S, Madhu G (2015) Investigation of structural and electrical properties of novel CuO–PVA nanocomposite films. *J Mater Sci* 50:7064–7074
28. Kocjan A, Logar M, Shen Z (2017) The agglomeration, coalescence and sliding of nanoparticles, leading to the rapid sintering of zirconia nanoceramics. *Sci Rep* 7(1):159
29. Peng Z, Kong L (2007) A thermal degradation mechanism of polyvinyl alcohol/silica nanocomposites. *Polym Degrad Stab* 92:1061–1071
30. Pasha S, Deshmukh K, Ahamed M, Chidambaram K, Mohanapriya M, Raj N (2015) Investigation of microstructure, morphology, mechanical, and dielectric properties of PVA/PbO nanocomposites. *Adv Polym Tech* 36:352–361
31. Rajesh K, Crasta V, Rithin Kumar N, Shetty G, Rekha P (2019) Structural, optical, mechanical and dielectric properties of titanium dioxide doped PVA/PVP nanocomposite. *J Polym Res* 26(4):69
32. Galil AA, Ali HE, Balboul MR (2015) Nano-ZnO doping induced changes in structure, mechanical and optical properties of PVA films. *Arab J Nucl Sci Appl* 48:77–89
33. Mahendia S, Tomar A, Kumar S (2010) Electrical conductivity and dielectric spectroscopic studies of PVA–Ag nanocomposite films. *J Alloys Compd* 508:406–411

Publisher's Note Springer Nature remains neutral with regard to jurisdictional claims in published maps and institutional affiliations.

Affiliations

V. Parthasarathy¹ · J. Selvi¹ · P. Senthil Kumar² · R. Anbarasan³ · S. Mahalakshmi⁴

¹ Department of Physics, Hindustan Institute of Technology and Science, Padur, Chennai, Tamil Nadu 603103, India

² Department of Chemical Engineering, SSN College of Engineering, Kalavakkam, Chennai, Tamil Nadu 603110, India

³ Department of Chemical Engineering, National Taiwan University, Taipei 10617, Taiwan

⁴ Department of Physics, Anand Institute of Higher Technology, Kazhipattur, Chennai, Tamil Nadu 603103, India